

Tailored Nickel Base Multilayer Systems with Adjusted Grain Size and Chemical Composition

Jutta Luksch,* Johannes Niegisch, Maike Jordt, Marion Weissenberger, Christoph Pauly, Florian Schaefer, and Christian Motz

Metal multilayers exhibit improved material properties in a wide range of applications. Used as coatings, they can make a component more resistant to wear or corrosion in particular environments. Multilayer coatings can also be used to add additional properties to a component and make it multifunctional. The fabrication and characterization of multilayers are therefore an important issue. Herein, both the fabrication and characterization of Ni/Cu and nano-crystalline/coarse-grained Ni (nc/cg-Ni) multilayers are presented. The production by means of electrodeposition also allows a variation of layer thicknesses from a few nanometers up to a few hundred micrometers and is easily scalable to industrial application. This article describes the single-bath deposition and analyzes the microstructure and composition of the homogeneously deposited Ni/Cu and nc/cg-Ni multilayers. A modulation of hardness in nc/cg-Ni varying from 4.9 to 6.1 GPa is achieved while the elastic modulus is nearly constant. In Ni/Cu multilayers, hardness varies from 6.4 to 6.1 GPa in the Ni- and Cu-rich layers, respectively. Additionally, the reduced Young's modulus ranges from 187.2 (Ni-rich) to 169.8 GPa (Cu-rich). The layer interfaces in both sample types are tested using microbending cantilevers and are found to be pore-free, mechanically stable and show crack-free plastic deformation.

1. Introduction

Multilayers of different materials or different microstructures of one material have enhanced material properties due to the synergies of material properties and can lead to new properties, e.g., giant magneto-resistance. Improved hardness,^[1] toughness,^[2] and reduced wear^[3,4] or improved corrosion resistance^[5] are reported in the literature. As a result, multilayers are used in many products, including roller and ball bearings, cutting tools, and car wheels.^[6] One reason for the improved mechanical properties is a potentially evolving size effect as layer thicknesses decrease. A size effect on yield stress and tensile strength in multilayers with grain size modulation in a NiCo alloy is described. Many thin coarse grain interlayers lead to a deviation from the mixing law above a certain interfacial density.^[7] A size effect in the hardness of multilayers of two different materials has been found in the way that lower layer thicknesses resulted in higher hardness, for instance.^[8–10]

Furthermore, an intrinsic size effect arises from the effect of grain size on plastic deformation behavior. Down to a grain size of about 1 μm , this is described as the well-known Hall–Petch effect where yield strength and hardness increase with $1/d^{(1/2)}$ and is caused by dislocation pile-up at grain boundaries causing a backstress on dislocation sources inside the grain. In the sub-micrometer regime, this trend is still observed, but the exponent can deviate from $-1/2$ due to an increasing role of the grain boundaries (GBs). As grain size decreases, innergranular dislocation sources become scarce and GBs can act as dislocation sinks or even transmit dislocations. Plastic deformation can become dominated by GB sliding, rotation, or migration rather than dislocation movement as grain sizes decrease to 10–20 nm. Hardness decreases due to the so-called inverse Hall–Petch effect. For a comprehensive treatment, the reader is referred to the review by Pineau et al.^[11] As multilayers are composites, the interfacial cohesion is crucial for mechanical behavior.^[12–14]

There are several top-down and bottom-up processes for producing multilayers. The most important of these is briefly described here. Top-down processes include accumulated roll bonding with achievable individual layer thicknesses of a few micrometers and below, where the challenge is to achieve consistent, homogeneous multilayer structures.^[13,15,16] There are

J. Luksch, J. Niegisch, M. Jordt, M. Weissenberger, F. Schaefer, C. Motz
Materials Science and Methods
Saarland University
66123 Saarbruecken, Germany
E-mail: j.luksch@matsci.uni-saarland.de

C. Pauly
Chair of Functional Materials
Saarland University
66123 Saarbruecken, Germany

C. Pauly
CoMiTo
Saarland University
66123 Saarbruecken, Germany

 The ORCID identification number(s) for the author(s) of this article can be found under <https://doi.org/10.1002/adem.202402331>.

© 2025 The Author(s). Advanced Engineering Materials published by Wiley-VCH GmbH. This is an open access article under the terms of the Creative Commons Attribution License, which permits use, distribution and reproduction in any medium, provided the original work is properly cited.

DOI: 10.1002/adem.202402331

also bottom-up processes such as physical vapor deposition (PVD)^[17] and chemical vapor deposition (CVD).^[17,18] These vacuum processes can achieve total layer thicknesses of up to several 100 μm (CVD) and nanoscale individual layer thicknesses (PVD preferred). A special CVD process is atomic layer deposition, which offers high thickness control but can only produce layers of a few 100 nm.^[19,20] An industrially established and cost-effective process is electrochemical deposition (ED).^[6,21] Ions dissolved in an electrolytic bath are deposited at the cathode by the flow of electric current. In ED, the microstructure can be specifically adjusted by using additives and tuning the current parameters, e.g., from direct current to pulsed current (PC) and reverse PC (RPC).^[22] The grain size of the deposit is determined by the concurrent processes of nucleation and growth. These, in turn, can be influenced by the overvoltage. At high overvoltage, nucleation is favored due to a rapid accumulation of atoms, but the starvation of ions in front of the cathode can lead to the outgrowth of individual grains, which in turn favors grain growth. This phenomenon is known as mass transport-controlled growth. At very low overpotentials the adatoms have enough time to assume a favorable energetic position at a growth edge through surface diffusion instead of contributing to the formation of new grains, so that larger grains are favored here.^[23] In the present study, pulsed electrodeposition (PED), ED with PC, is used.

With ED, multilayers can, in principle, be produced by two different methods,^[24] either by changing the electrolyte (two-bath synthesis)^[25] or by changing the deposition parameters such as current, stirring,^[26] temperature, and so on (single-bath synthesis)^[27] to change composition and structure. In two-bath synthesis, the variety of electrolytes available^[28] and the robustness of the deposition parameters are an advantage, while the interface between the layers can be a weak point (e.g., due to oxide formation during sample transfer from bath 1 to bath 2 and vice versa^[24]), which can affect the desired multilayer properties. In industrial large-scale applications, a change of electrolyte is hard to achieve because of large volume, causing cross-contamination, and so on. One disadvantage of single-bath synthesis is the limited choice of electrolytes available for the different combinations of metal ions. Examples of possible combinations are Co/Cu,^[29] Sn/Cu,^[30] and NiFe/Cu^[31] as well as Ni/Cu.^[32,33] Deeper insight is given in ref. [6]. In addition to the two-bath synthesis of Ni/Cu by Lamovec et al.^[34] Agarwal et al.^[35] produced Ni/Cu alloy layers by single-bath synthesis with different compositions but inhomogeneous microstructures. Xue and Zhang report on the microstructure and tribological properties of Ni/Cu multilayers from single-bath synthesis with a maximum individual layer thickness of 300 nm and a total layer thickness of 8 μm .^[32,33]

As described above, to the best of the authors' knowledge, there is little literature on the production of Ni/Cu or nanocrystalline/coarse-grained (nc/cg) multilayers with PED. In addition, the interface of the coatings has rarely been explicitly investigated mechanically. In this work, the production of Ni/Cu, i.e., material variation, and nc/cg-Ni, i.e., microstructure variation, by means of PED is presented. The microstructure of the produced multilayer systems is characterized by scanning electron microscope (SEM) backscatter electron (BSE) images and energy-dispersive X-ray spectroscopy (EDS) as well as transmission

electron microscope (TEM). Furthermore, the mechanical properties of the individual layers are measured by nanoindentation. The mechanical properties of the interfaces are analyzed using microcantilever samples in situ SEM.

2. Experimental Section

2.1. Material Manufacturing

2.1.1. Electrodeposition Setup

All electrodepositions were carried out in a double-walled glass vessel of 1.5 L. The glass vessel was constantly supplied with 50 °C hot water via a circulation thermostat (Julabo ED-5, JULABO GmbH, Seelbach, Germany). For continuous filtration of the electrolyte, a filter (KL 13 OF, Mahle Aftermarket GmbH, Stuttgart, Germany) was used via a pump (NF 100 KT.18s, KNF DAC GmbH, Hamburg, Germany) with a downstream pulsation damper. The electrodes and the stirring unit (DSMP320-12-51-BF, MSW Motion Control GmbH, Werther (Westf.), Germany) were attached to an adapted lid of the container to ensure the reproducibility by a constant setup and resulted in a vertical deposition geometry. Deposition was galvanostatic, with a function generator (WW 5061, Taboer Electronics Ltd., Nesher, Israel) defining the pulse shape, which was then amplified by a galvanostat (Wenking HP 96, Bank Elektronik—Intelligent Controls GmbH, Pohlheim, Germany). The variation of the pulse parameters for multilayer deposition was carried out via a MATLAB (The MathWorks Inc., Natick, United States) control of the function generator.

For all depositions, a cathode with an area of 30 mm by 30 mm made of 2 mm thick copper sheet was used, which was rounded at the edges and ground to a grain size of 4000 SiC grinding paper. Cleaning was carried out with isopropanol. For nc/cg-Ni deposition, the anode, referred to as Ni pellets (Ampere GmbH, Schönebeck, Germany) in the table below, consisted of a basket made of expanded Ti metal in which the pellets were held and contacted with the galvanostat. A semipermeable dialysis tube (VISKING-Membra-Cell, RCT Reichelt Chemietechnik GmbH + Co., Heidelberg, Germany) was placed around the basket to keep particles that were produced when the pellets were dissolved away from the electrolyte. Pt-coated expanded metal was used as an insoluble anode for the Cu-containing deposits.

2.1.2. Electrolyte

A nickel sulfamate electrolyte^[36] was used as the basis. The exact compositions for the Ni/Cu and nc/cg-Ni electrolytes can be found in **Table 1**.

Nickel sulfamate (Enthone, 185 g L⁻¹ Ni) served as ion source. Boric acid (CHEMSOLUTE, $\geq 99.8\%$, 10043-35-3) was used as a pH buffer; sodium dodecyl sulfate (SDS, AppliChem GmbH, $\geq 99.5\%$, 151-21-3) as a surfactant and saccharin sodium salt dihydrate (Merck KGaA, $\geq 99.0\%$, for synthesis, 6155-57-3) and 2-butyne-1,4-diol (Merck Schuchardt OHG, $\geq 99.0\%$, (not stabilized) for synthesis, 110-65-6) were additives for grain refinement and brightening. For the nc/cg-Ni deposition, nickel chloride hexahydrate (VWR, $\geq 98\%$, 7791-20-0) promoted the

Table 1. Composition of the two different electrolytes used.

Component	Concentration	
	nc/cg-Ni	Ni/Cu
Nickel sulfamate [mL L ⁻¹]	595	595
Boric acid [g L ⁻¹]	35	35
Nickel chloride [g L ⁻¹]	5	–
SDS [g L ⁻¹]	0.2	0.2
Copper sulfate [g L ⁻¹]	–	4
Sodium saccharin [g L ⁻¹]	0.18	1
Butynediol [g L ⁻¹]	0.02	–

dissolution of the Ni pellets. Copper sulfate pentahydrate (Grüssing GmbH, ≥99.0%, 7758-99-8) served as copper ion source for the Ni/Cu deposition. The ingredients were completely dissolved in distilled water at 50 °C before the electrolyte was filled into the deposition vessel via filtration. The pH value for the deposition of pure Ni layers was kept in the range of 2.9–3.2 by adding amidosulfuric acid (Merck KGaA, ≥99.0%, for synthesis, 5329-14-6). For the Cu-containing deposits, an initial pH value of 3.8 was used and the electrolyte was discarded when as the pH value fell below 2.9.

2.1.3. Deposition Parameter

An overview of the deposition parameters for the various material compositions and microstructures is given in **Table 2**. The temperature of the electrolyte during all depositions was held at 50 °C and the bath was stirred. Growth rates of 2.03 nm min⁻¹ for nc-Ni, 18.52 nm min⁻¹ for cg-Ni, 2.67 nm min⁻¹ for Ni-rich, and 0.49 nm min⁻¹ for Cu-rich layers were achieved based on the deposition parameters. For the nc/cg-Ni multilayers, a high overpotential was chosen in order to achieve a cg structure via mass transport-controlled growth. As nc parameter set, the current–time curve from previous work^[36,37] was optimized with regard to the lower saccharin content (from 45 to 40 mA cm⁻²). The off time prevented excessive starvation of the ions in front of the cathode and thus mass transport-controlled growth.

To modulate the composition of the Ni/Cu multilayers, the current density was varied, with Ni-rich deposits forming at a higher current density and a Cu-rich deposit at a lower current density, as shown in the literature.^[38] The lower current density corresponded to a lower potential at which the reduction of the nobler copper ions was increased relative to nickel ions. In a

Table 2. Deposition parameters for nc/cg-Ni and Ni/Cu multilayers.

Electrolyte [-]	Layer [-]	Anode material [-]	Stirring [rounds min ⁻¹]	Current density I_{on} [mA cm ⁻²]	t_{on} [ms]	t_{off} [ms]
nc/cg-Ni	nc-Ni	Ni pellets	32	40	5	10
nc/cg-Ni	cg-Ni	Ni pellets	32	120	1	–
Ni/Cu	Ni-rich	Pt	20	45	5	10
Ni/Cu	Cu-rich	Pt	20	5	5	10

current–potential curve, the deposition reactions of the different compositions were assigned to different potential ranges. These ranges were influenced by the ion concentrations and their ratios. For galvanostatic deposition, these potential ranges must also be assigned to different current ranges, which can be set using the parameters mentioned above. In preliminary work for this article, the relevant current density range was narrowed down to 5–45 mA cm⁻² using a parameter study, for the Cu-rich and Ni-rich, respectively.

2.2. Material Characterization

The characterization of the layer systems was carried out in the central area of the cathodes during the parameter study to identify the effective parameters in **Table 2**. This guarantees that edge effects during deposition were excluded. An edge region of about 2 mm formed a slightly thicker deposit due to a higher current density at the edges. Thus, all investigations were carried out with a distance of at least 5 mm to the edge.

2.2.1. Composition and Microstructure

The composition, microstructure, and layer thickness distribution were characterized along the horizontal central axis of the substrate at intervals of 5 mm over a distance of 20 mm. The cross sections were metallographically prepared by grinding with SiC paper, polishing with diamond suspensions of grain sizes 3 and 1 μm, and finally polishing with colloidal oxide suspension. For final polishing, OP-S NonDry 0.25 μm (Struers GmbH, Willich, Germany) was used for the nc/cg-Ni layers and OP-U NonDry 0.04 μm (Struers GmbH, Willich, Germany) for the Ni/Cu layers both using a fine polishing cloth ChemoMet (Buehler, ITW Test & Measurement GmbH European Headquarters, Leinfelden-Echterdingen, Germany) for 4 min.

The microstructure of all samples was examined using BSE images in the SEM (Sigma VP, Carl Zeiss IQS Deutschland GmbH, Oberkochen, Germany). BSE images were used to exclude possible defects and to ensure preparation artefacts from the focused ion beam (FIB) liftout in the TEM. The compositions of the Cu-containing deposits were measured by EDS (Oxford Instruments, Abingdon, UK) at 20 kV using a line profile along the direction of growth. For high-resolution inspection in the nanocrystalline layers, TEM lamellas were prepared using Xe-PFIB (Xe PFIB, Helios PFIB G4 CXe, Thermo Fisher Scientific Inc., Waltham, United States), for Ni/Cu multilayer or Gallium FIB (Ga FIB, Helios NanoLab600, FEI, Hillsborow, United States), for nc/cg-Ni multilayer liftout, which are, however, limited to a few individual layers. Quantitative grain size determination of nc/cg samples was done using electron backscatter diffraction (Velocity Plus, EDAX LLC, Pleasanton, CA, United States) in the Xe-PFIB at 20 kV on a Xe-PFIB-polished cross section. Patterns were recorded and postprocessed in OIM Analysis 9 using the NPAR (Neighboring Pattern Averaging and Reindexing) algorithm followed by spherical indexing to account for the low pattern quality in the nc layers. In the Ni/Cu samples, the grains were even smaller so that a transmission Kikuchi diffraction (TKD) measurement with 10 nm step size was performed on the TEM lamella at 30 kV high

voltage and 45° sample tilt as a compromise between detector signal and lateral resolution. Again, postprocessing via NPAR and spherical indexing was applied to improve indexing rate. The Ni/Cu lamella was placed on an Mo liftout grid to improve the validity of EDS measurements. Particular attention was paid to the layer transitions. TEM investigations were performed in a thermal field emission microscope (JEM-F200, JEOL (Germany) GmbH, Freising, Germany) at 200 kV equipped with a dual EDS detector system (JEOL (Germany) GmbH, Freising, Germany) used for compositional line scans and element mappings in scanning TEM (STEM) mode. Microstructure imaging in TEM was done using an STEM bright-field (BF) detector.

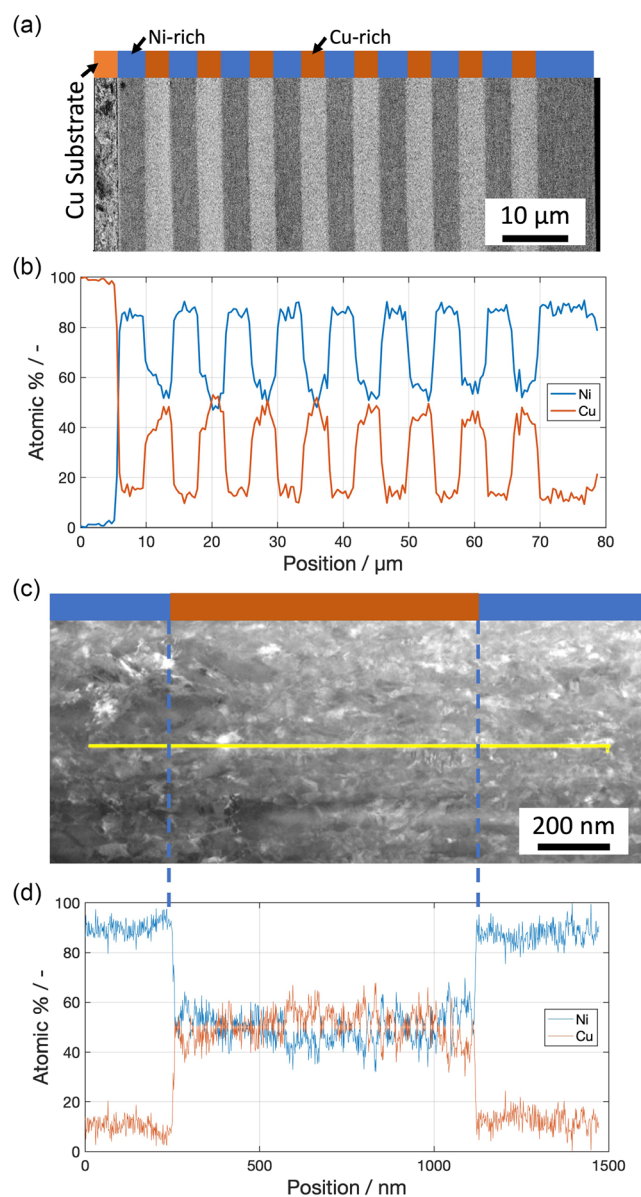


Figure 1. Result of a 4 μm Ni/Cu layer system. a) SEM BSE image with recognizable fine-grained microstructure, b) corresponding EDS line data, c) STEM BF image of a layer transition to characterize the interface, and d) EDS line data of the TEM sample from (c) showing the sharp transition within the layers.

2.2.2. Hardness and Young's Modulus

The hardness and the reduced modulus of elasticity were determined using nanoindentation (TI 980, Bruker Corporation, Billerica, United States) with a diamond Berkovich tip (Synton-MDP AG, Nidau, Switzerland). A grid of 6 × 25 indentations was measured over a range of 9 μm × 37.5 μm. The load was applied in force open loop control up to about 2 mN maximum force. This means that the deformation zone for expected indents in a metal with 200 GPa modulus of elasticity and 6 GPa hardness is small enough compared to the grid spacing of 2 μm, so that no influence of the indents on each other is expected. The indentation grid was rotated by 5–10° relative to the multilayers to ensure a uniform distribution of indents in the layers of about 4 μm single layer thickness.

2.2.3. Mechanical Properties of Interface

As described in the introduction, special attention must be paid to the layer interfaces. The mechanical properties were tested in this work by means of quasistatic bending of microcantilevers with a cross-sectional $B \times W$, of about 12 μm × 12 μm and lever arm of 40 μm. The microcantilevers were produced using FIB on sample edges that had been ground and polished finally with 1 μm diamond polishing suspension. The interface to be tested was placed in the area of the highest stress and was localized and increased by a notching. The cantilevers were tested in situ in the SEM using a nanoindenter (Alemnis, Thun, Switzerland) and a wedge tip for uniform force application. The indenter performed displacement-controlled at a speed of 50 nm s⁻¹, so that a

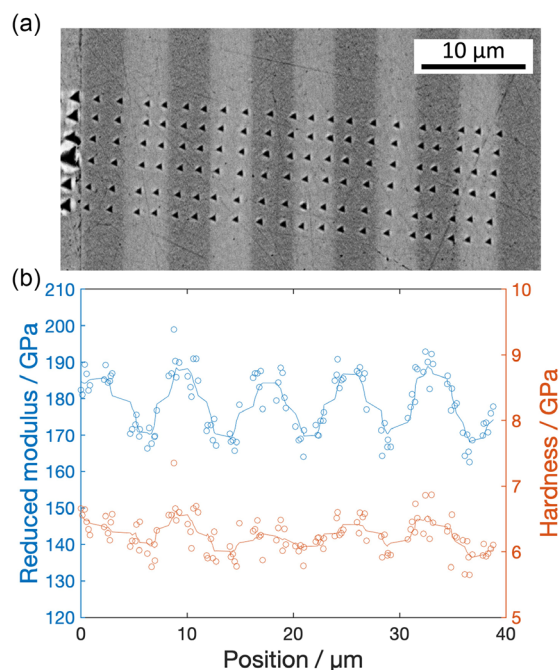


Figure 2. Results of the nanoindentation measurements for Ni/Cu multilayer a) SEM BSE image of the test position and b) hardness and Young's modulus along the layer system. A moving average filter is added as a guide to the eye.

quasistatic test of the interface was performed. Unloading segments made it possible to determine the stiffness, which could be used to detect possible crack growth. To analyze the local deformation, the interface was imaged in the SEM and examined using FIB cross sections.

3. Results and Discussion

The microstructure of the layers across the width of the substrate is qualitatively homogeneous, whereby the absolute layer thicknesses at a distance of 10 mm from the center are $\approx 28\%$ higher (Ni/Cu) and 37% higher (nc/cg-Ni) due to the electric field elevation toward the edge. The higher current applied to the cg layers tends to enhance this effect. Due to the comparable microstructure, only the results from the center area of the substrate are shown below.

3.1. Ni/Cu Multilayer

3.1.1. Composition and Microstructure

A layer system with 4 μm single layer thickness is shown in Figure 1a. Here, deposition was carried out alternately with a

current density of 45 and 5 mA cm^{-2} (see Table 2). According to an EDS line scan, the composition varies between 10 and 15 and just under 50 at% Cu content in the layers, respectively (Figure 1b). The microstructure is shown in higher resolution in Figure 1c, where no clear layer interface can be seen. Note the absence of growth defects at the interface, e.g., pores or oxide layers. Due to the small difference in average atomic number, compositional contrast in STEM imaging is essentially absent. High-resolution TEM imaging was affected by a large amount of lattice defects, grain boundaries and diffraction contrast, which obstruct possible compositional contrast. Nevertheless, an STEM EDS line scan shows a sharp transition between the layers within 7 nm (Figure 1d). The grain size in the TEM lamella was measured with TKD with a maximum of the grain size distribution between 60 and 100 nm. This is in the range of grain size-induced hardening rather than softening (inverse Hall–Petch effect), due to GB moderated flow as known for very small grain-sized nanocrystalline materials. In nickel, the transition from Hall–Petch effect to inverse Hall–Petch effect occurs around 15 nm grain size.^[39]

3.1.2. Hardness and Reduced Modulus

Figure 2a shows an SEM BSE image of the nanoindentation measurement of the Ni/Cu layer sample starting at the substrate.

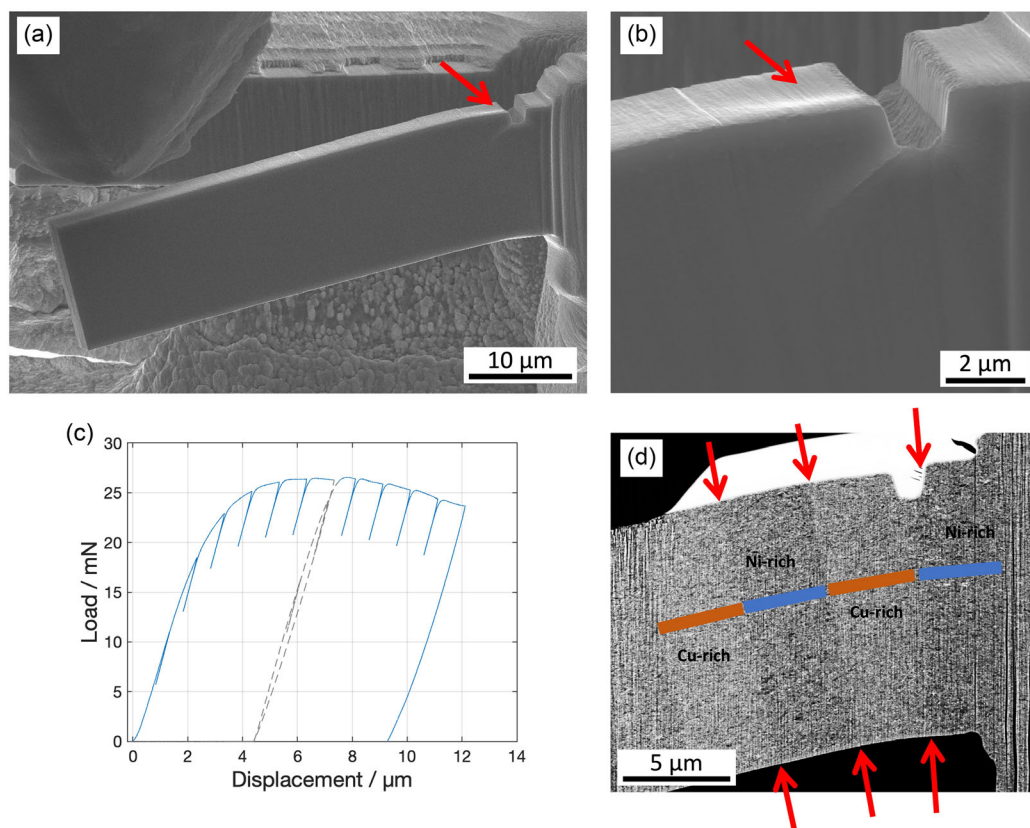


Figure 3. a) Ni/Cu cantilever and wedge tip illustrating the geometry of the quasistatic bending experiment. b) Detail of the cantilever after bending showing the transition from FIB-cut notch to actual deformation and plastic deformation on the front face. Red arrows in (a,b) indicate the area of local deformation which takes place mainly in the Cu-rich layer. c) Corresponding load–displacement curve including unloading segments shows pronounced plastic deformation and constant stiffness. d) SEM BSE image of a FIB cross section showing the position of the notch and pronounced deformation of the first Cu-rich layer. No layer delamination can be seen. Red arrows indicate the position of the interfaces.

The corresponding values of hardness and reduced modulus are shown in Figure 2b. The reduced modulus shows a clear variation across the layers in a range of 169.8 GPa (Cu-rich layer) and 187.2 GPa (Ni-rich layer). In contrast, the hardness varies much less between 6.1 and 6.4 GPa. Based on the Young's modulus of the pure metals nickel (205 GPa) and copper (130 GPa) and layer composition of Ni90Cu10 and Ni50Cu50, the measured values are in good agreement with the rule of mixtures. The high hardness values are caused by the Hall–Petch effect due to small grain sizes.

3.1.3. Mechanical Properties of Interface

The mechanical strength of the interface between the Ni-rich and Cu-rich layers was tested quasistatically along the layers as shown in Figure 3. Figure 3a shows the cantilever tested with a wedge indenter with a notch at the transition from a Ni-rich to a Cu-rich layer. Local deformation and necking can be seen in the Cu-rich layer to the left-hand side of the notch (Figure 3b red arrow). The force–displacement curve with unloading segments is shown in Figure 3a and shows elastic–plastic behavior without spontaneous force drops that would indicate brittle failure. A postmortem FIB cross section indicates that the plastic deformation was mainly carried by the Cu-rich layer (Figure 3d) which is in good

agreement with the lower hardness measured in Cu-rich layer. No interface failure can be detected.

3.2. nc/cg-Ni Multilayer

3.2.1. Microstructure

The microstructure of the pure Ni coating was characterized using BSE in the SEM, as shown in Figure 4a,b. A uniform and homogeneous thickness of the layers is observed without larger defects such as pores. The layer transitions from nc to cg appears smoother than the transitions from cg to nc, although the resolution in the SEM is not sufficient to resolve the grain structure. Therefore, a TEM lamella was examined in the STEM for a closer look at the layer transitions (Figure 4c,d). The STEM BF images confirm the impressions from the SEM images. In addition, the difference in grain size between the layers becomes quantifiable. The observations suggest that the uneven transitions are a consequence of the direction of growth. The cg layer forms a rougher surface, which is levelled by a subsequent nc layer. Furthermore, a clear difference in grain size can be observed in the layers. The grains in the cg layers are columnar in the growth direction with a mean minimum Feret diameter of 0.819 μm and a small spread and a wide spread

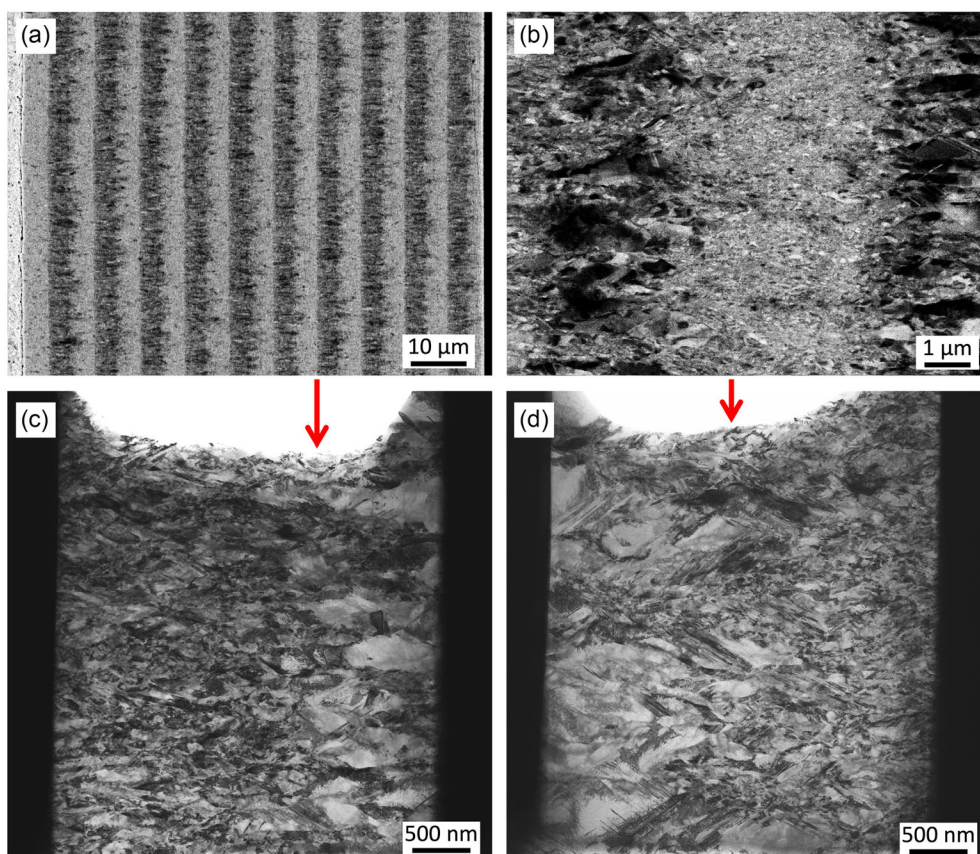


Figure 4. a) SEM BSE overview of the nc/cg-Ni multilayer showing homogeneous thickness distribution and a total thickness of about 80 μm . nc-Ni layers are the light gray and the cg-Ni layers are the dark gray layers. b) Detail of the layer interfaces in SEM BSE mode shows rougher transition from cg to nc. STEM BF images showing c) a smooth nc to cg transition and d) a rough cg to nc transition. Red arrows indicate the approximate location of the interfaces. Both types of interface are free from growth defects. Growth direction from left to right.

maximum Feret diameter without a clear maximum from 0.334 to 6.455 μm whereas the finer grained layer has grains with mean diameter of 0.263 μm .

3.2.2. Hardness and Young's Modulus

Figure 5a shows an SEM BSE image of the nanoindentation measurement of the nc/cg-Ni layer sample starting at the substrate. The corresponding values of hardness and reduced modulus are shown in **Figure 5b**. The reduced modulus varies between 190 and 210 GPa with an average value of 202.9 GPa. A slight variation with grain size can be recognized. Possible causes are different texture states in connection with the elastic anisotropy of nickel and the higher volume fraction of grain boundaries in the nc layers. Furthermore, a difference in grain-size-dependent deformation mechanisms could lead to a different height of material pile-up around the indents in the two layers. In general, a difference in H/E ratio as observed here is a hint for that. A larger pile-up results in a larger contact area which affects the calculation of the reduced modulus that could be origin of the observed small oscillations. The hardness, on the other hand, varies significantly across the layers with values of 4.9 GPa in the cg layers and 6.1 GPa in the nc layers. This variation is in good qualitative agreement with the Hall–Petch law. The absolute values are fully consistent with published data for nc-Ni by Maier et al.^[40] and Yang and Vehoff.^[41]

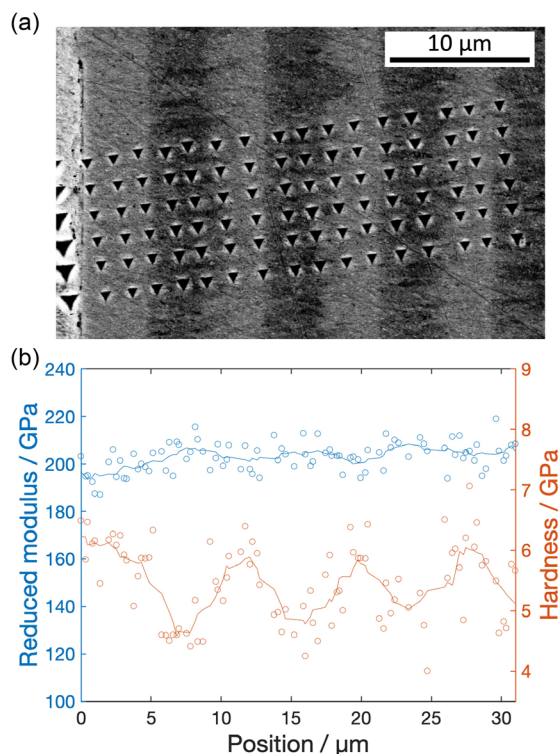


Figure 5. Results of the nanoindentation measurements for nc/cg-Ni multilayer. a) SEM image of the test position and b) hardness map Young's modulus map line diagram. A moving average filter is added as a guide to the eye.

3.2.3. Mechanical Properties of Interface

Here, the mechanical stability of the nc/cg-Ni layer system was tested quasistatically. **Figure 6a,b** shows a cantilever with notch at the transition from cg to nc layer before the test. **Figure 6c** shows the force–displacement curve of the quasistatic bending with unloading segments. The curve shows a pronounced elastic–plastic deformation of the cantilever without a load drop that would indicate brittle failure; the unloading segments show no change in the cross section and thus no crack growth. To confirm this, the cantilever was polished after the test using FIB and imaged in BSE contrast (**Figure 6d**). The plastic opening of the notch without cracking is clearly visible which is typical for microbending experiments due to size effect. Furthermore, the cg layer to the left-hand side of the notch shows necking, which means that the yield stress was exceeded at this point, reflecting the lower hardness in cg. The deformation in the cg layer takes place via dislocation nucleation, dislocation movement in the grains, dislocation interactions with the GBs, and GB movement, for example, whereas in the nc layer the volume fraction of GBs is higher and the movement of the dislocations is more limited, for example, due to backstress from the boundaries. The result shows that the interface from cg-Ni to nc-Ni does not represent a mechanical weak point.

3.3. Comparison of Multilayer Systems

An alternation in hardness and Young's modulus could be achieved. The Ni-rich layer of the Ni/Cu system is similar to the nc layer of the nc/cg-Ni system in terms of microstructure, hardness, and Young's modulus. The higher saccharin content leads to smaller grains which fits well to the measured grain sizes in the different layers and possible texture effects can explain the slight difference.

A difference can be seen in the transition of the layers. The material variation shows no microstructural jump or effect at the transition from Cu- to Ni-rich and from Ni- to Cu-rich layer, whereas the transition from nc to cg layer is very planar and from cg to nc layer follows the contour of the large grains. For the Ni/Cu multilayers, the clear interface can be explained by the similarity of the lattice parameters of Cu and Ni, with a change of layers within the grains. On the other hand, the rough interface in nc/cg-Ni multilayer of cg to nc layer is related to the growth front of the ED, because the cg layer has a rough growth front with a matt surface, while the nc layer has a smooth growth front and therefore a shiny/reflective surface. This behavior could possibly be adjusted with RPC technology and thus a pulsed partial dissolution, especially of the protruding roughness of the uppermost layer.^[22] For the global mechanical properties, there are initially no signs of major effects of the uneven layer transitions.

A limiting factor for the achievable total layer thickness on a laboratory scale results from the small cathode surface area of 30 \times 30 mm^2 , which leads to electric field peaks at the edges and therefore uneven thickness distribution over longer deposition times. In addition, the limited electrolyte volume of 1.5 L and the lack of conditioning on a laboratory scale are critical for depositing thicker layers. However, both limitations can be easily overcome on an industrial scale, enabling deposition of total layer

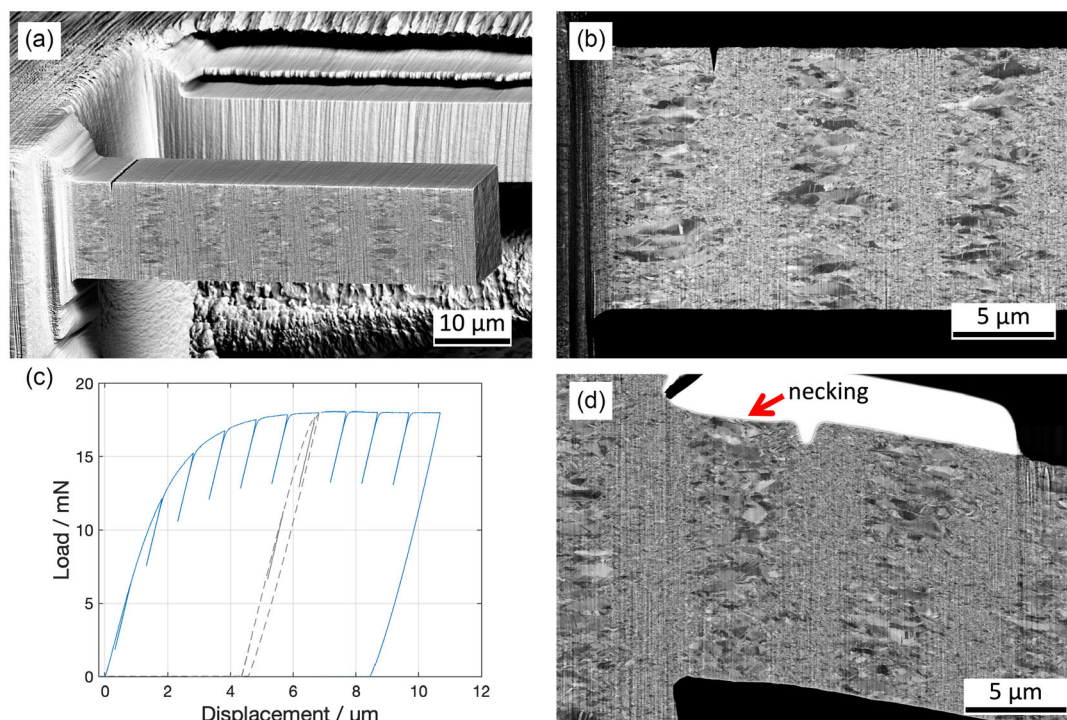


Figure 6. a) SEM BSE image of a nc/cg-Ni cantilever after FIB milling. b) Detail of the cantilever from (a) in notch region. c) Corresponding load–displacement curve including unloading segments shows pronounced plastic deformation and constant stiffness. d) SEM BSE image FIB cross section showing the position of the notch and pronounced deformation of the cg-Ni layer. No layer delamination can be seen.

thicknesses in the order of millimeters with individual layer thicknesses from a less than a micrometer up to several hundred micrometers. A limitation could be the presence of residual growth stresses, although nc-Ni single layers of 2 mm thickness could already be produced on a laboratory scale without any problems. No unusually high residual stress (bending of the lamella) was observed in the TEM sample preparation by FIB liftout in this study, indicating that the deposition parameters chosen here could be suitable for thicker layers.

4. Conclusion

Single-bath PED was used to produce multilayer systems with compositional variation (Ni/Cu) and with microstructure variation (nc/cg-Ni): 1) Ni/Cu multilayers show a sharp transition from 10 to 15 at% Cu to ≈ 50 at% Cu content. nc/cg-Ni multilayers make the transition from cg to nc more complex due to large grains. 2) Ni/Cu multilayers show a reduced modulus ranging from 169.8 GPa for Cu-rich layers to 187.2 GPa for Ni-rich layers. nc/cg-Ni multilayers exhibit hardness from 4.9 GPa for cg layers to 6.1 GPa for nc layers. 3) The interfaces in both multilayer systems are pore-free, mechanically stable, and show ductile and crack-free behavior in microbending.

This confirmed the positive effects of deposition from single-bath synthesis on the interface cohesion and successfully established the deposition method. Further variation of the current parameters and deposition conditions of the Ni/Cu system could produce an even greater difference in Young's modulus and thus

further overall property variation. Furthermore, it is conceivable to vary both hardness and Young's modulus in a layer system through a combined material and microstructure variation, which would further extend the possible property variations of the layer systems.

From another point of view, this fabrication route allows the intrinsic size effect to be studied in fatigue tests using the methods described in refs. [42,43].

Acknowledgements

The TEM was funded by “Europäischer Fonds für regionale Entwicklung” (EFRE) as part of the operational program EFRE Saarland 2014–2020 under the objective “Investitionen in Wachstum und Beschäftigung.” This work made use of the resources of the Correlative Microscopy and Tomography (CoMiTo) core facility at Saarland University. Funding by Deutsche Forschungsgemeinschaft (DFG) for project funding 521371248, the Plasma-FIB/SEM (415217285), and the Nanoindenter (497801977) is greatly acknowledged. Funding for the in situ Nanoindenter from federal state Saarland is greatly acknowledged.

Open Access funding enabled and organized by Projekt DEAL.

Conflict of Interest

The authors declare no conflict of interest.

Author Contributions

Jutta Luksch: conceptualization (equal); data curation (lead); formal analysis (lead); investigation (lead); methodology (equal); project

administration (lead); supervision (supporting); visualization (lead); writing—original draft (lead). **Johannes Niegisch**: investigation (supporting); writing—review and editing (supporting). **Maik Jordt**: investigation (supporting); writing—review and editing (supporting). **Marion Weissenberger**: investigation (supporting); writing—review and editing (supporting). **Christoph Pauly**: conceptualization (supporting); investigation (supporting); methodology (supporting); writing—review and editing (equal). **Florian Schaefer**: funding acquisition (lead); investigation (equal); methodology (supporting); project administration (supporting); supervision (equal); writing—review and editing (equal). **Christian Motz**: conceptualization (equal); project administration (lead); resources (lead); supervision (equal); writing—review and editing (equal).

Data Availability Statement

The data that support the findings of this study are available from the corresponding author upon reasonable request.

Keywords

interface mechanical properties, multilayer fabrication, nanoindentation, pulsed electrodeposition

Received: October 4, 2024

Revised: January 7, 2025

Published online: February 7, 2025

- [1] B. Postolnyi, V. Beresnev, G. Abadias, O. Bondar, L. Rebouta, J. Araujo, A. Pogrebnyak, *J. Alloys Compd.* **2017**, 725, 1188.
- [2] T. Koseki, J. Inoue, S. Nambu, *Mater. Trans.* **2014**, 55, 227.
- [3] M. Allahyarzadeh, M. Aliofkhaezai, A. S. Rouhaghdam, H. Alimadadi, V. Torabinejad, *Surf. Coat. Technol.* **2020**, 386, 125472.
- [4] C. S. K. Ghosh, P. K. Limaye, R. Tewari, *Trans. IMF* **2010**, 88, 158.
- [5] M. Allahyarzadeh, M. Aliofkhaezai, A. S. Rouhaghdam, V. Torabinejad, H. Alimadadi, A. Ashrafi, *Electrochim. Acta* **2017**, 258, 883.
- [6] M. Aliofkhaezai, F. C. Walsh, G. Zangari, H. Köçkar, M. Alper, C. Rizal, L. Magagnin, V. Protsenko, R. Arunachalam, A. Rezvani, A. Moein, S. Assareh, M. H. Allahyarzadeh, *Appl. Surf. Sci. Adv.* **2021**, 6, 100141.
- [7] M. Daly, S. Haldar, V. K. Rajendran, J. McCrea, G. D. Hibbard, C. V. Singh, *Mater. Sci. Eng., A* **2020**, 771, 138581.
- [8] M. Wang, D. Wang, T. Kups, P. Schaaf, *Mater. Sci. Eng., A* **2015**, 644, 275.
- [9] J. P. H. A. Misra, H. Kung, *Philos. Mag. A* **2002**, 82, 2935.
- [10] R. Hoagland, R. Kurtz, C. Henager, *Scr. Mater.* **2004**, 50, 775.
- [11] A. Pineau, D. L. McDowell, E. P. Busso, S. D. Antolovich, *Acta Mater.* **2016**, 107, 484.
- [12] F. Liang, H.-F. Tan, B. Zhang, G.-P. Zhang, *Scr. Mater.* **2017**, 134, 28.
- [13] X. Ma, C. Huang, J. Moering, M. Ruppert, H. W. Höppel, M. Göken, J. Narayan, Y. Zhu, *Acta Mater.* **2016**, 116, 43.
- [14] H. Liu, B. Zhang, G. Zhang, *Scr. Mater.* **2011**, 64, 13.
- [15] P. M. Pohl, M. Kuglstatler, M. Göken, H. W. Höppel, *Metals* **2023**, 13, 1049.
- [16] Y. Sun, Y. Chen, N. Tsuji, S. Guan, *J. Alloys Compd.* **2020**, 819, 152956.
- [17] I. Shishkovsky, P. Lebedev, *Nanocoatings and Ultra-Thin Films*, Woodhead Publishing Series in Metals and Surface Engineering (Eds: A. S. H. Makhlof, I. Tiginyanu), Woodhead Publishing **2011**, pp. 57–77, <https://doi.org/10.1533/9780857094902.1.57>.
- [18] K. Choy, *Prog. Mater. Sci.* **2003**, 48, 57.
- [19] J. Zhang, Y. Li, K. Cao, R. Chen, *Nanomanuf. Metrol.* **2022**, 5, 191.
- [20] C. W. Wiegand, R. Faust, A. Meinhardt, R. H. Blick, R. Zierold, K. Nielsch, *Chem. Mater.* **2018**, 30, 1971.
- [21] I. Gurrappa, L. Binder, *Sci. Technol. Adv. Mater.* **2008**, 9, 043001.
- [22] M. Chandrasekar, M. Pushpavanam, *Electrochim. Acta* **2008**, 53, 3313.
- [23] A. J. Brad, L. R. Faulkner, H. S. White, *Electrochemical Methods*, John Wiley and Sons Ltd., Hoboken, NJ, USA **2022**.
- [24] C. A. Ross, *Annu. Rev. Mater. Res.* **1994**, 24, 159.
- [25] A. Haseeb, J. Celis, J. Roos, *J. Electrochem. Soc.* **1994**, 141, 230.
- [26] R. Engelken, H. McCloud, *J. Electrochem. Soc.* **1985**, 132, 567.
- [27] B. Bahadormanesh, M. Ghorbani, N. L. Kordkolaei, *Appl. Surf. Sci.* **2017**, 404, 101.
- [28] F. C. Walsh, *Trans. IMF* **2022**, 100, 233.
- [29] B. Tóth, L. Péter, I. Bakonyi, *J. Electrochem. Soc.* **2011**, 158, D671.
- [30] F. C. Walsh, C. Low, *Trans. IMF* **2016**, 94, 152.
- [31] S. Esmaili, M. E. Bahrololoom, C. Zamani, *Surf. Eng. Appl. Electrochem.* **2011**, 47, 107.
- [32] W. Zhang, Q. Xue, *Thin Solid Films* **1997**, 305, 292.
- [33] Q. Xue, W. Zhang, *J. Phys. D: Appl. Phys.* **1997**, 30, 3301.
- [34] J. Lamovec, V. Jović, I. Mladenović, M. Sarajlić, V. Radojević, in *2014 29th Int. Conf. on Microelectronics Proc. - MIEL 2014*, Belgrade, Serbia **2014**, pp. 183–186, <https://doi.org/10.1109/MIEL.2014.6842116>.
- [35] M. Agarwal, V. Kumar, S. Malladi, R. Balasubramaniam, K. Balani, *JOM* **2010**, 62, 88.
- [36] K. Schueler, B. Philippi, M. Weinmann, V. M. Marx, H. Vehoff, *Acta Mater.* **2013**, 61, 3945.
- [37] D. Rathmann, M. Marx, C. Motz, *J. Mater. Res.* **2017**, 32, 4573.
- [38] T. Miyake, M. Kume, K. Yamaguchi, D. P. Amalnerkar, H. Minoura, *Thin Solid Films* **2001**, 397, 83.
- [39] Y.-R. Jeng, P.-C. Tsai, S.-H. Chiang, *Wear* **2013**, 303, 262.
- [40] V. Maier, K. Durst, J. Mueller, B. Backes, H. W. Höppel, M. Göken, *J. Mater. Res.* **2011**, 26, 1421.
- [41] B. Yang, H. Vehoff, *Acta Mater.* **2007**, 55, 849.
- [42] J. Luksch, A. Lambai, G. Mohanty, F. Schaefer, C. Motz, *Mater. Sci. Eng., A* **2023**, 884, 145452.
- [43] J. Luksch, A. Lambai, G. Mohanty, C. Pauly, F. Schaefer, C. Motz, *Mater. Des* **2024**, 241, 112880.